High-Performance Optical 3R Regeneration for Scalable Fiber Transmission System Applications

Zuqing Zhu, *Student Member, IEEE*, Masaki Funabashi, Zhong Pan, *Student Member, IEEE*, Loukas (Lucas) Paraschis, *Member, IEEE*, David L. Harris, *Member, IEEE*, and S. J. Ben Yoo, *Fellow, IEEE*, *Fellow, OSA*

***Abstract*—This paper proposes and demonstrates optical 3R regeneration techniques for high-performance and scalable 10-Gb/s transmission systems. The 3R structures rely on monolithically integrated all-active semiconductor optical amplifier-based Mach–Zehnder interferometers (SOA-MZIs) for signal reshaping and optical narrowband filtering using a Fabry–Pérot filter (FPF) for all-optical clock recovery. The experimental results indicate very stable operation and superior cascadability of the proposed optical 3R structure, allowing error-free and low-penalty 10-Gb/s [pseudorandom bit sequence (PRBS) $2^{23}-1$] return-to-zero (RZ) transmission through a record distance of 1 250 000 km using 10 000 optical 3R stages. Clock-enhancement techniques using a SOA-MZI are then proposed to accommodate the clock performance degradations that arise from dispersion uncompensated transmission. Leveraging such clock-enhancement techniques, we experimentally demonstrate error-free 125 000-km RZ dispersion uncompensated transmission at 10 Gb/s (PRBS $2^{23}-1$) using 1000 stages of optical 3R regenerators spaced by 125-km large-effective-area fiber spans. To evaluate the proposed optical 3R structures in a relatively realistic environment and to investigate the tradeoff between the cascadability and the spacing of the optical 3R, a fiber recirculation loop is set up with 264- and 462-km deployed fiber. The field-trial experiment achieves error-free 10-Gb/s RZ transmission using PRBS $2^{23}-1$ through 264 000-km deployed fiber across 1000 stages of optical 3R regenerators spaced by 264-km spans.**

***Index Terms*—All-optical clock recovery, clock enhancement, dispersion uncompensated transmission, Fabry–Pérot filter (FPF), field trial, optical regeneration, semiconductor optical amplifier-based Mach–Zehnder interferometer (SOA-MZI), synchronous modulation, wavelength conversion.**

I. Introduction

WHILE THE remarkable growth of Internet traffic has spurred intensive research on efficient and scalable optical network systems, the major technical difficulties for improving transmission system scalability are still the physical layer limitations from signal-to-noise ratio degradation, chromatic dispersion (CD), and other impairment mechanisms. Compared to the O/E/O counterpart, optical-regeneration technology can potentially work with lower power consumption and much more compact size and can provide transparency to protocol and format [1]–[4]. It is well known that the optimal bit error rate (BER) of a regenerated signal is the same as that before the regeneration if measured directly after the regenerator [5], [6]. Consequently, single-stage optical-regeneration measurements at the output of the regenerator may show improved eye diagrams but do not show improved system performance [2]. Inline cascaded optical-regeneration experiments are necessary to reveal the benefit of optical regeneration by maintaining low BER through the cascaded regeneration stages and to estimate the ultimate cascadability of the optical regenerators. Previous studies have demonstrated 3600-km dispersion uncompensated transmission at 2.5 Gb/s using nine stages of optical 2R regeneration [4], 1 000 000-km transmission at 40 Gb/s over 2500 3R stages with electrical clock recovery [7], [8], 10 000-km transmission at 40 Gb/s using 65 stages of optical 3R with all-optical clock recovery [9], and 200 000-km transmission at 10 Gb/s using 1430 stages of optical 3R with electrical clock recovery [10]. However, only a few of these works included all-optical clock recovery to improve optical transparency, and none included cascaded optical 3R regeneration for uncompensated fiber transmissions at 10 Gb/s. Also, all of these works set up the fiber recirculation loops with well-controlled lab fiber spools, which have relatively stable characteristics compared to deployed field-fiber spans. In this paper, we propose and demonstrate optical 3R regeneration techniques relying on monolithically integrated all-active semiconductor optical amplifier-based Mach–Zehnder interferometers (SOA-MZIs) for signal reshaping and a Fabry–Pérot filter (FPF) for all-optical clock recovery. Together with a simple all-optical clock-enhancement technique, the optical 3R techniques achieve stable operation for both dispersion-compensated and uncompensated transmissions using one physical setup with only minor changes. The 10-Gb/s experiments demonstrate error-free operations of 1 250 000-km return-to-zero (RZ) transmission using pseudorandom bit sequence (PRBS) $2^{23}-1$ across 10 000 optical 3R stages and 125 000-km RZ dispersion uncompensated transmission using PRBS $2^{23}-1$ through 1000 optical 3R stages that are spaced by 125-km large-effective-area fiber (LEAF). We also performed 3R recirculation loop experiments employing field-fiber links and achieved 264 000-km error-free field transmission for 10-Gb/s RZ input signals using PRBS $2^{23}-1$ with a 3R regeneration spacing of 264 km.

The rest of the paper is organized as follows. Section II presents the experimental and simulation investigation on the limitations of SOA-MZI-based optical 2R regeneration.

Manuscript received May 12, 2006; revised September 29, 2006.

Z. Zhu, M. Funabashi, Z. Pan, and S. J. B. Yoo are with the Department of Electrical and Computer Engineering, University of California, Davis, CA 95616 USA (e-mail: yoo@ece.ucdavis.edu).

L. Paraschis is with the Optical Networking Advanced Technology Group, Cisco Systems, San Jose, CA 95134 USA (e-mail: loukas@cisco.com).

D. L. Harris is with the Advanced Technology Labs of Sprint together with Nextel, Burlingame, CA 94010 USA (e-mail: David.L2.Harris@sprint.com).

Digital Object Identifier 10.1109/JLT.2006.888256

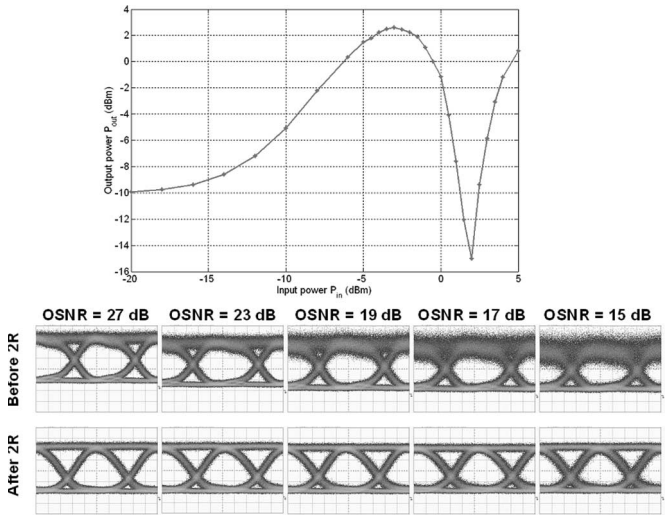

Fig. 1. Power transfer function of a SOA-MZI and the input/output eye diagrams of optical 2R regeneration.

Section III discusses the enabling techniques for the proposed all-optical 3R regenerators, such as timing realignment with synchronous modulation and all-optical clock recovery utilizing an FPF. Section IV proposes and demonstrates the optical 3R regeneration techniques for dispersion compensate/uncompensated RZ signals. It further investigates the all-optical clock-enhancement technique to obtain superior cascadability of these 3R structures. Section V discusses the field-trial experiment of the optical 3R regeneration techniques. Finally, Section V summarizes this paper.

II. Optical 2R Regeneration Using SOA-MZI

The interferometric property of a SOA-MZI provides a nonlinear power transfer function for suppressing the amplitude noise. Fig. 1 plots the static power transfer function of an integrated all-active SOA-MZI. The optical 2R regeneration experiment takes optical signals with different optical signal-to-noise ratios (OSNRs) and reshapes them using SOA-MZI operating in the logic-inverting mode [1]. The original signals are at 10 Gb/s with $2^{31}-1$ PRBS. Fig. 1 shows the input and output eye diagrams for input OSNR values ranging from 15 to 27 dB on a 0.1-nm resolution bandwidth. The eye diagrams indicate that SOA-MZI-based optical 2R regeneration effectively suppresses amplitude noise and provides cleaner space and mark levels. One drawback of SOA-MZI-based optical 2R regeneration is that it accompanies increases in timing jitter. The intrinsic speed limitation of interband carrier recombination processes in SOAs induces high-frequency pattern-dependent timing jitter [11], while amplified spontaneous emission (ASE) noise generated in the active regions induces wideband Gaussian-like (white-noise) timing jitter [12], [13]. Fig. 2 shows the experimental results for cascaded operation of 1–3 SOA-MZIs in the logic-inverting mode. The back-to-back signal is 10 Gb/s using PRBS $2^{31}-1$. The output eye diagrams in Fig. 2(a) indicate jitter accumulations through the cascaded operation of the SOA-MZIs. The phase margins at 10^{-9} BER, which are obtained by measuring the BER when sweeping the sampling position, are 64, 61, 52, and 25 ps for the back-to-back, first, second, and third stages, respectively. Fig. 2(b) shows the jitter spectral analysis results (100 kHz–5 GHz, normalized to the total signal power) for the cases of back to back and after the third stage. The pattern dependence of the SOA-MZIs generates jitter spectral peaks at 714 kHz, 1.43 MHz, and 2.14 MHz, etc., and the SOA ASE noise raises the background jitter noise floor.

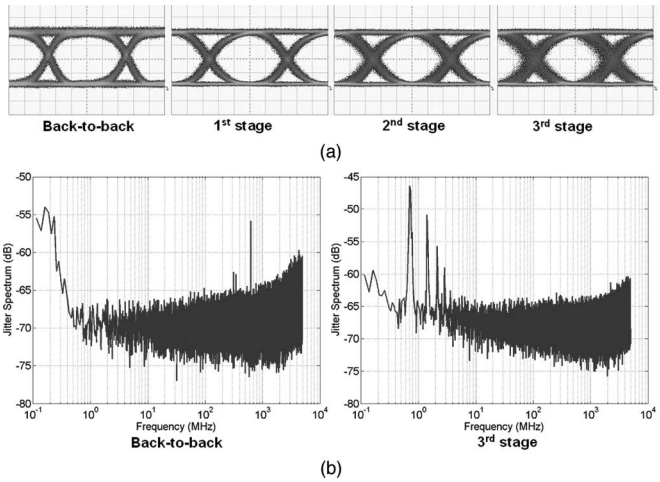

Fig. 2. Experimental results of cascaded operations of SOA-MZIs. (a) Eye diagrams. (b) Jitter spectral analysis results.

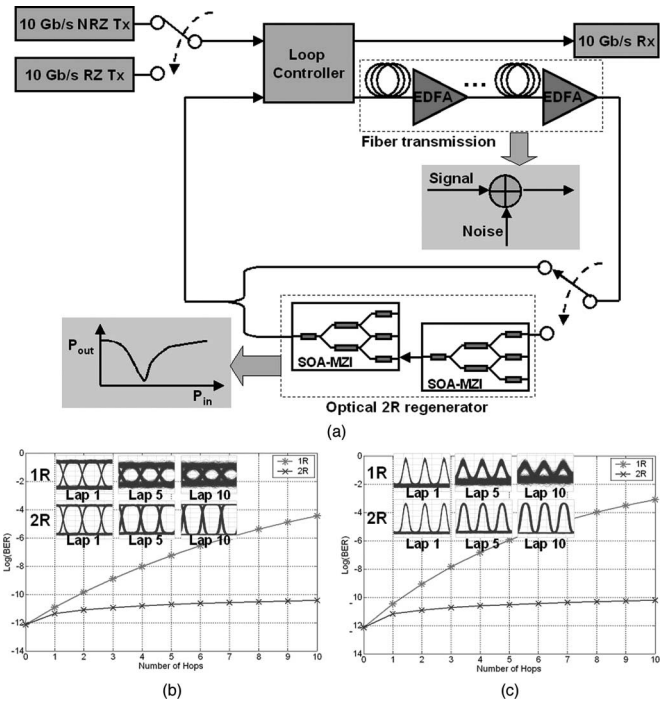

Fig. 3. (a) Simulation configuration for cascaded optical 2R regeneration using SOA-MZIs, Tx—transmitter, Rx—receiver, EDFA—erbium-doped fiber amplifier. (b) NRZ simulation results. (c) RZ simulation results.

We performed simulations to further investigate the amplitude noise suppression performance of such optical 2R regenerators in a situation that isolates the jitter effects. The simulations utilize an analytical model similar to that in [5]. As shown in Fig. 3(a), the optical 2R regenerator built with two cascaded SOA-MZIs operating in the inverting mode is inline

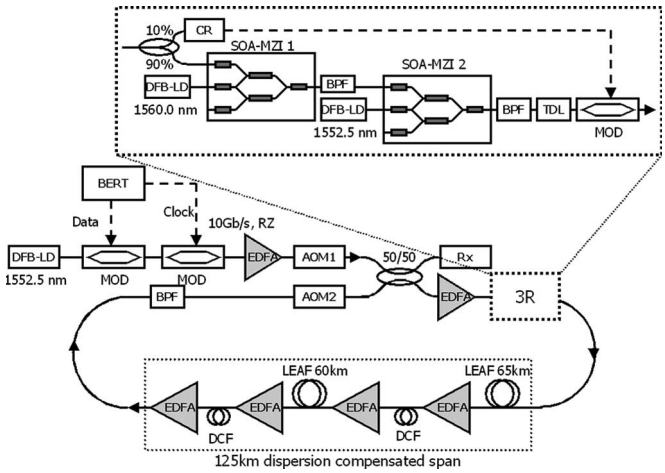

Fig. 4. Experimental setup of in-line optical 3R regeneration with electrical clock recovery: BERT—bit-error-rate tester; DFB-LD—DFB laser diode; CR—electrical clock recovery; BPF—optical bandpass filter; MOD—$LiNbO_3$ modulator; EDFA—erbium-doped fiber amplifier; DCF—dispersion compensating fiber; AOM—acoustic optical modulator; Rx—optical receiver.

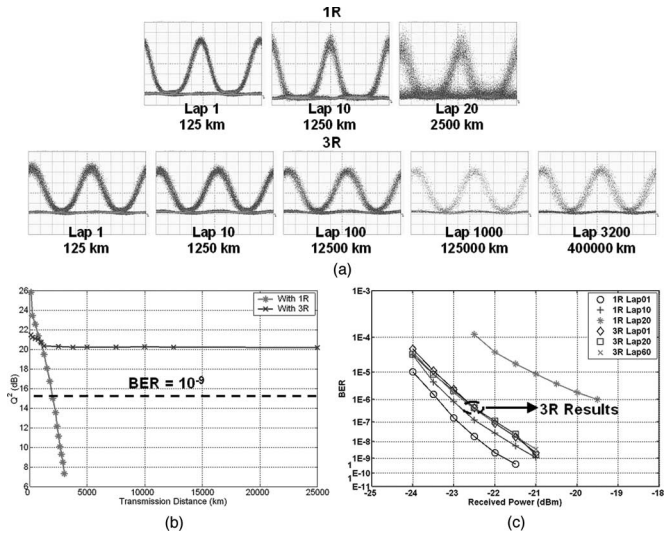

Fig. 5. (a) Eye diagrams of 1R and 3R regeneration outputs. (b) Q-factor evolutions with transmission distance for 1R and 3R regeneration. (c) BER measurement results for 1R and 3R regeneration.

with the fiber transmission, which is modeled as erbium-doped fiber amplifiers (EDFAs) and attenuators, where the addition of ASE noise with Gaussian distribution (white noise) takes place. The simulation models the optical 2R regenerator with the normalized power transfer function in Fig. 1. Both non-RZ (NRZ) and RZ modulation format cases have been simulated for comparing two transmission systems with and without optical 2R regeneration. As Fig. 3(b) and (c) indicates, for both the NRZ and RZ cases, the BER increases nearly exponentially as the hop count increases because of rapid amplitude noise accumulations in the 1R scheme, while the in-line optical 2R regenerator suppresses such BER increases with the hop count by limiting the amplitude noise after each regeneration stage.

Experimental and simulation results shown in Figs. 2 and 3 both indicate that SOA-MZI-based optical 2R regeneration can effectively suppress the amplitude noise from accumulating at each stage. On the other hand, the timing jitter accompanying the 2R process limits the cascadability of such optical 2R regenerators. To suppress such timing-jitter accumulations, additional regeneration by retiming must be added to 2R regeneration. The following sections discuss several optical 3R regeneration technologies.

III. Enabling Techniques for All-Optical 3R Regeneration

A. Timing Realignment Using Synchronous Modulation

Synchronous modulation remodulates the recovered clock onto the reshaped optical signal through optoelectronic or all-optical modulation [2]. This scheme decouples the reshaping and the retiming functions and simplifies the system optimization. Fig. 4 shows the experimental setup of optical 3R regeneration utilizing synchronous modulation with an O/E converter and an $LiNbO_3$ modulator [15]. The BER tester (BERT) generates a 10-Gb/s data stream using $2^{23}-1$ PRBS. The two $LiNbO_3$ modulators in sequence imprint data and clock onto the DFB laser emission and produce a 10-Gb/s optical RZ signal at 1552.5 nm. The fiber recirculation loop consists of two fiber spans with a total length of 125-km (65 + 60 km) LEAF fiber with dispersion compensation. The optical 3R regenerator includes the reshaping stage consisting of two SOA-MZIs in cascaded operation. The retiming stage takes the electrical clock from a 10-GHz electrical clock-recovery module (Agilent 83434A) for synchronous modulation. The tunable delay line aligns the timing of the data to the recovered clock.

As shown in Fig. 5(a), the eye diagrams of the 3R regenerated signal show clear opening even after 3200 loops (0.4 million-km transmission). The eye diagrams of the 1R-regenerated signal (EDFA only without 3R) indicate strong jitter and amplitude noise accumulations only after 20 loops (2500-km transmission). Fig. 5(b) and (c) plots the Q-factor and BER measurement results. The Q-factor of the 1R case falls below 15.5 dB $(\text{BER} = 10^{-9})$ after 16 loops, while the Q-factor of the 3R case stabilizes at approximately 20.3 dB after 200 loops. There is no appreciable power penalty between Laps 1, 20, and 60 in the case of 3R regeneration. The 1R case shows a 0.8-dB penalty between Laps 1 and 10 at BER 10^{-9}, and the curve for Lap 20 has a BER error floor around 10^{-6}. The experimental results indicate that retiming using synchronous modulation greatly improves the cascadability of optical regeneration based on SOA-MZIs.

B. All-Optical Clock Recovery Using FPF

The FPF-based all-optical clock recovery [16], [17] relies on the narrowband optical filtering to extract the clock components in the signal spectrum [18]. Fig. 6(a) shows the 10-Gb/s all-optical clock-recovery module built with an FPF and a gain-saturated SOA [16]. The FPF has a free spectral range (FSR) of 10 GHz and a finesse of 100. Fig. 6(b) shows the signal measured directly after the FPF with 10-Gb/s RZ input signals with $2^{31}-1$ PRBS. The signal contains periodic optical clock pulses with frequency matching to the FPF's FSR (i.e., data clock). Significant pattern-dependent amplitude variations still

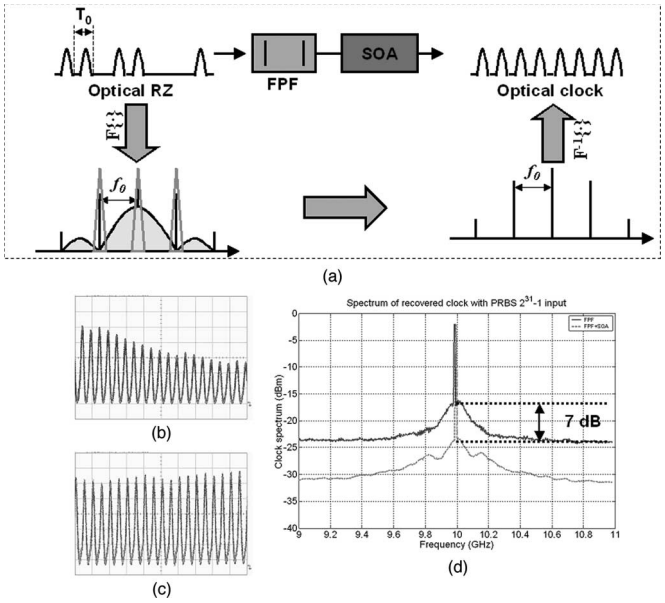

Fig. 6. (a) All-optical clock-recovery setup based on an FPF and a SOA. (b) Recovered clock after the FPF with PRBS $2^{31}-1$ input. (c) Recovered clock after the FPF and the SOA with PRBS $2^{31}-1$ input. (d) RF spectra of the recovered clocks.

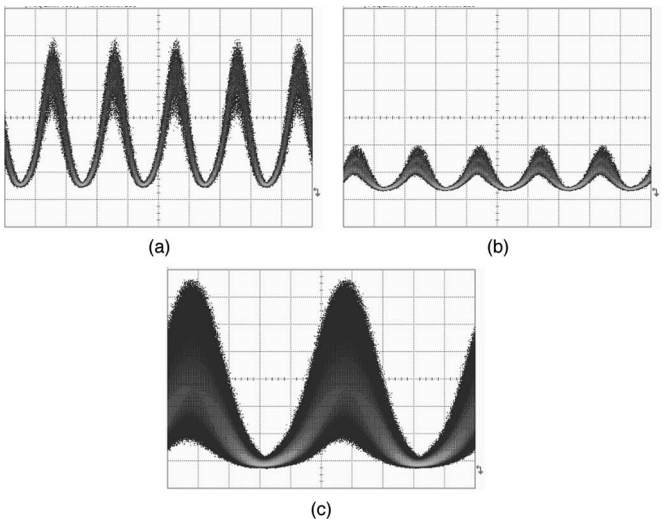

Fig. 7. Polarization dependence of the FPF-based clock recovery. (a) Best polarization input (50 ps/div). (b) Worst polarization input (50 ps/div). (c) Clock recovered from signal after 125-km fiber transmission (20 ps/div, persisted for 30 min).

exist because the amplitude can decay when long sequences of repeated zeros occur [18]. The gain-saturated SOA reduces these amplitude variations by limiting amplification [as shown in Fig. 6(c)]. Fig. 6(d) shows the RF spectrum comparison of the recovered clocks with and without a gain-saturated SOA, indicating that the latter case increases the side-lobe suppression ratio of the clock signal by 7 dB.

Polarization sensitivity, if any, in fiber FPFs may cause unwanted drift in the spectral response of the filter as the input polarization state varies. Fig. 7(a) and (b) shows the 10-GHz recovered clocks at the "best" and "worst" (highest and lowest power throughput cases for the given signal) polarization states of the FPF when the device temperature is stabilized at

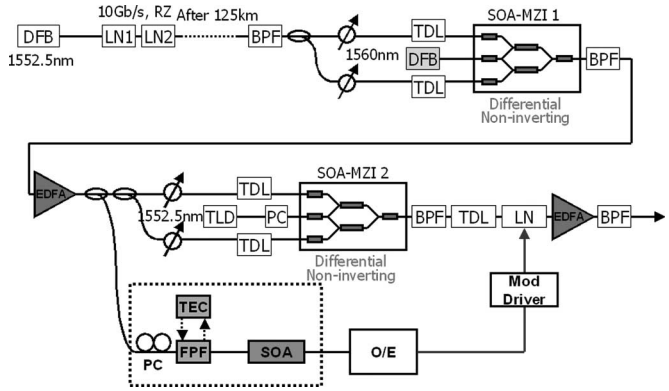

Fig. 8. Experimental setup of 10-Gb/s optical 3R regenerator with FPF-based all-optical clock recovery. DFB—DFB laser diode; LN—$LiNbO_3$ modulator; PC—polarization controller; TEC—temperature control loop; O/E—optical-to-electrical converter; Mod Driver—modulator driver.

18.55 °C using an external temperature control loop. There are approximately 6-dB amplitude variations. Fig. 7(c) shows the 10-GHz clock recovered from the signal experienced 125-km LEAF fiber transmission on a 30-min persisting screen display. Due to the polarization sensitivity of the commercial FPF, the field-fiber experiments, including the FPF-based all-optical clock recovery, show limited stability over this time scale.

IV. Optical 3R Regeneration Experiments Using Lab Fiber

A. Optical 3R Regeneration for RZ Signals

Fig. 8 shows the setup of the 10-Gb/s optical 3R regenerator with FPF-based all-optical clock recovery [16]. The reshaping stage consists of two SOA-MZIs operating in the differential mode with 35-ps relative delay between the two interferometric arms. The SOA-MZI pair operating in cascade preserves the wavelength and enhances the nonlinearity in the regenerative power transfer function [19]. The retiming stage incorporates the FPF-based all-optical clock recovery and the synchronous modulation using an $LiNbO_3$ modulator. The first SOA-MZI removes the signal polarization variations from fiber transmission with polarization-insensitive wavelength conversion. The recovered optical clock drives an O/E converter and a modulator driver that supplies a synchronous-modulation clock signal to the $LiNbO_3$ modulator for retiming.

The experiments evaluate the optical 3R regenerator in a fiber recirculation loop including 125-km LEAF fiber with dispersion compensation (as shown in Fig. 4). The 10-Gb/s signal has a PRBS pattern length of $2^{23}-1$. Fig. 9(c) shows the eye-diagram evolution from 3R Lap 10 to Lap 10 000. Clear eye openings can be observed at Lap 10 000 after 1 250 000-km transmission. Fig. 9(a) plots the Q-factor measurement up to 1000 loops. The Q-factor is stabilized above 22 dB with optical 3R regeneration. Fig. 9(b) shows the BER measurements at back to back and 3R Laps 1, 10, 100, 1000, and 10 000. There is less than 1-dB power penalty at 10^{-9} for transmission over 1 250 000 km relative to the back-to-back before transmission. All BER curve plots appear straight with no sign of error floors, and the BER values go below 10^{-9} at the received power of -21 dBm. To further explore the stability of the optical 3R

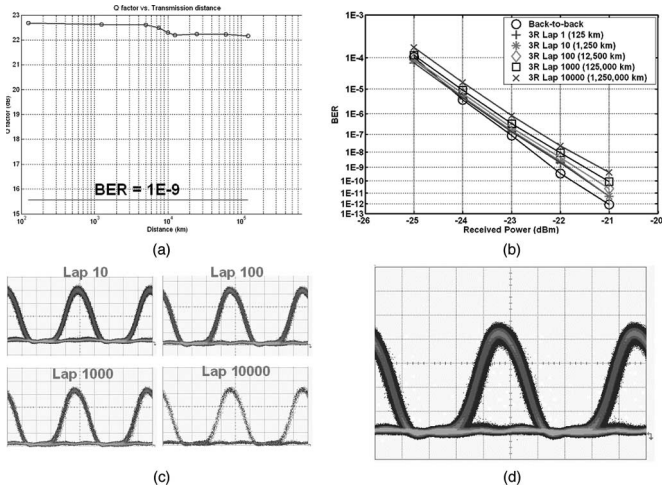

Fig. 9. Experimental results of 3R with all-optical clock recovery. (a) Q-factor versus transmission distance. (b) BER measurements. (c) 3R eye diagrams for Laps 10, 100, 1000, and 10 000. (d) Overlapping eye diagram of Laps 1 to 10 000 outputs (persisted for 10 min).

regeneration, we use free-run trigger instead of gated trigger to overlap the eye diagrams from Lap 1 to Lap 10 000. Fig. 9(d) shows a clear opening in the overlapped eye diagram recorded on a 10-min persisting display.

B. Optical 3R Regeneration for Dispersed RZ Signal

Fiber CD adds complexity to clock recovery due to the clock RF fading [20], [21]. RF fading strongly affects the performance of the clock-recovery technique based on narrowband filtering by attenuating the magnitude of the clock-frequency components. A small signal analysis provides the intensity of the clock component changing with the CD as [20]

$$\frac{I_L}{I_0} = \frac{\left|\cos\left(\frac{\pi\lambda^2 \mathrm{DL} f^2}{c} + \arctan(\alpha)\right)\right|}{\left|\cos\left(\arctan(\alpha)\right)\right|} \tag{1}$$

where I_L and I_0 are the clock intensity at distance 0 and L, respectively, DL is the total dispersion, f is the clock frequency, and α is the chirp parameter of the initial modulation. The RF fading induced by CD causes an intensity fluctuation of the recovered clock, and without preknowledge of the transmitter chirp α and the total dispersion DL, it is difficult to predict this intensity variation.

Completely uncompensated transmission is an extreme situation where the transmission system fully relies on the optical 3R regenerator for CD compensation. SOA-MZI-based optical 2R regeneration can reduce the amplitude domain distortion caused by CD [4]. To overcome CD-induced clock fading, we propose to include a clock-enhancement stage. Fig. 10 shows the proposed optical 3R structure. Fig. 10(a) shows the eye diagram of a 10-Gb/s RZ signal after uncompensated 125-km LEAF fiber transmission with a total CD of 531.25 ps/nm. The initial RZ pulses have an FWHM of 35 ps (PRBS $2^{23}-1$). The clock-enhancement stage includes an SOA-MZI in a push–pull operation. The SOA-MZI works in an over-modulated mode in which the device is driven across the minimum point on the transfer function to enhance the clock components [22]. Fig. 11

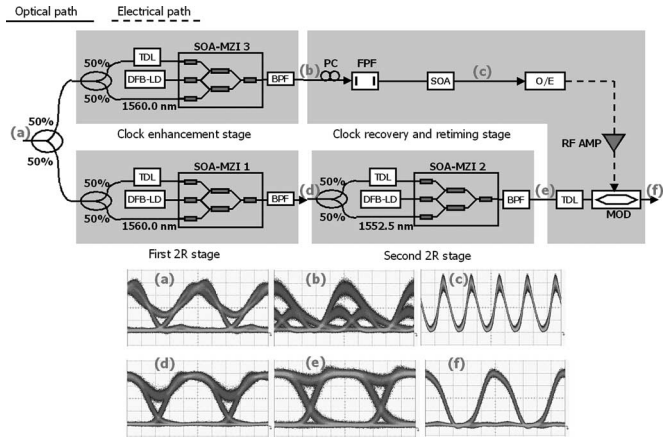

Fig. 10. Proposed structure of optical 3R regenerator for dispersion uncompensated RZ signals. RF AMP—RF amplifier.

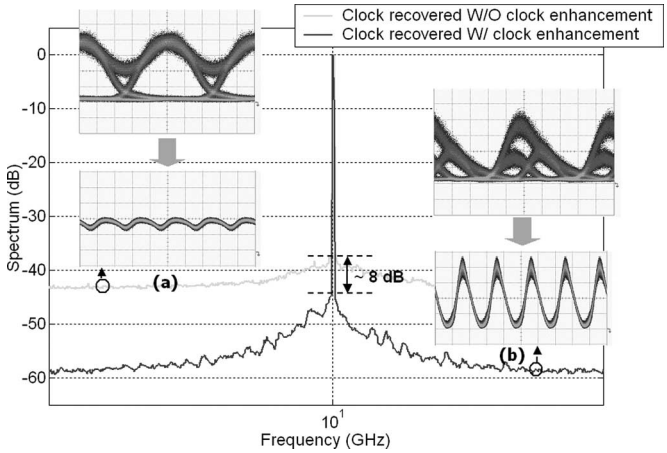

Fig. 11. RF spectrum comparison of the clocks recovered with and without clock enhancement. (a) Eye diagrams of clock recovery without clock enhancement. (b) Eye diagrams of clock recovery with clock enhancement.

shows the RF spectrum comparison of the clocks recovered with and without clock enhancement. The clock enhancement improves the clock side-lobe suppression ratio by 8 dB. As shown in Fig. 11(a), without clock enhancement, the recovered clock shows small amplitude and poor extinction ratio (< 3 dB) due to RF fading, while the clock enhancement provides a clean clock with an extinction ratio of 10 dB [as shown in Fig. 11(b)].

Fig. 12 shows the fiber recirculation loop experiment setup. The fiber loop consists of two uncompensated fiber spans with a total length of 125-km (65 + 60 km) LEAF fiber. The total CD of the fiber spans is 531.25 ps/nm at the operating wavelength 1552.5 nm. Fig. 12(a) plots the estimated dispersion curve of the fiber spans. Fig. 12(b) shows the eye-diagram evolution from Lap 1 to Lap 2000 (125–250 000-km uncompensated transmission). Clear eye opening can be obtained up to Lap 1000. Due to the fact that CD generates pattern-dependent distortions and that it affects the jitter suppression of the clock recovery, a small amount of jitter accumulates from Lap 1 to Lap 1000. At Lap 2000, the jitter accumulation generates dots inside the eye diagram. Fig. 12(c) plots the BER of signals at back to back and 3R Laps 1, 10, 100, 200, 500, 1000, and 2000 versus the average receiver power. There is only a 1.2-dB penalty at 10^{-9} for transmission over 125 000 km

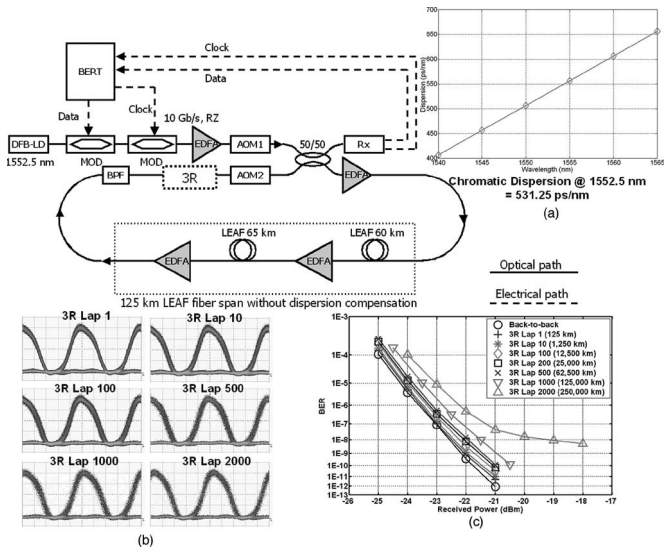

Fig. 12. Experimental setup of optical 3R regeneration for dispersion uncompensated RZ signals. (a) Estimated dispersion curve of the LEAF fiber spans. (b) 3R eye-diagram evolution. (c) BER measurements.

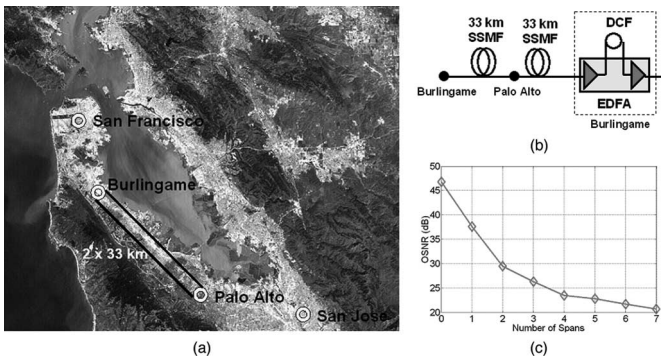

Fig. 13. (a) Field-fiber map. (b) Setup of one field-fiber span, SSMF—standard single-mode fiber, DCF—dispersion-compensation fiber, EDFA—erbium-doped fiber amplifier. (c) OSNR evolution through the fiber spans.

(Lap 1000) relative to the back-to-back before transmission. All BER curves are error-floor free, expect for the one at Lap 2000, which has an error floor at BER $\sim 10^{-8}$. This is from the residual jitter accumulation mentioned above. One possible solution to overcome this is to further stabilize the recovered clock using an active feedback control method.

V. Field Trials of Optical 3R Regeneration

While previous sections demonstrate optical 3R regeneration experiments in well-controlled lab environments, this section discusses the assessments of the 3R techniques under relatively realistic field-fiber conditions. We perform field-trial experiments by inserting the optical 3R regenerator in fiber recirculation loops built with deployed fiber links. Fig. 13(a) plots the map of the field fiber. Each field-fiber span consists of 66-km (2×33 km) standard single-mode-fiber (SSMF), which runs from Burlingame to Palo Alto, CA, and loops back. As indicated in Fig. 13(b), there are a two-stage EDFA and a DCF located at Burlingame to compensate for the loss and the CD of the fiber transmission. Fig. 13(c) shows the OSNR evolution through the fiber spans. The fiber recirculation loops are set

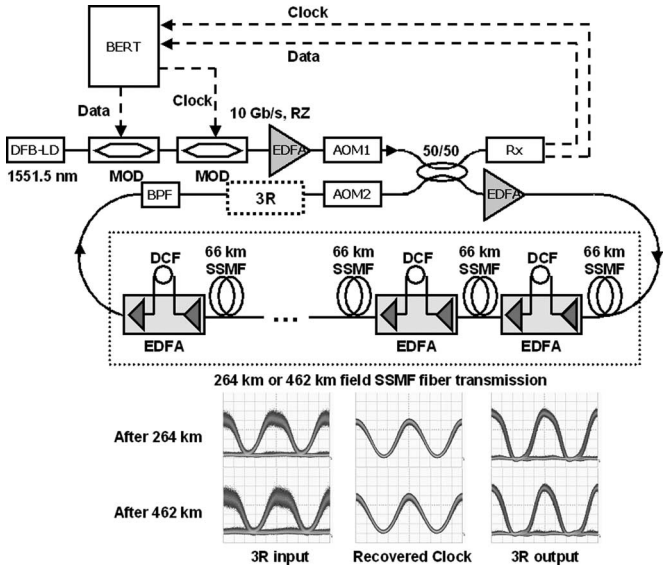

Fig. 14. Experimental setup of the field-trial experiments and eye-diagram measurements.

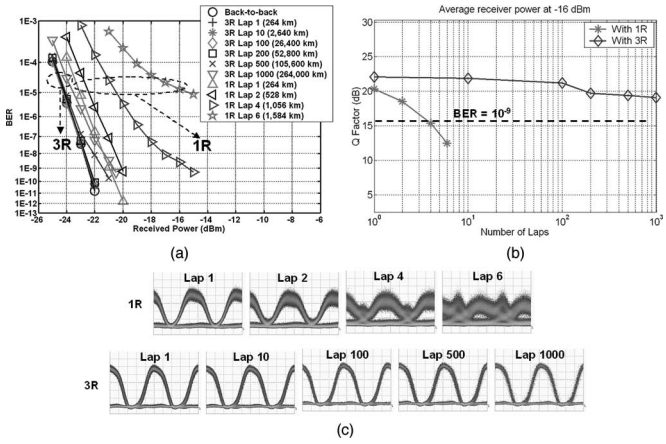

Fig. 15. Experimental results when loop length is 264 km. (a) BER curves. (b) Q-factor plots. (c) Eye diagrams.

up with four (264 km) or seven (462 km) field-fiber spans. The corresponding OSNRs after 264- and 462-km field transmission are 23.5 and 20.6 dB (0.1-nm resolution bandwidth), respectively. The residual CD is 26 ps/nm after 264 km and is 80 ps/nm after 462 km at the operating wavelength of 1551.5 nm. Fig. 14 shows the experimental setup. The optical transmitter generates a 10-Gb/s RZ signal using PRBS $2^{23} - 1$. The optical 3R regenerator has the same structure as illustrated in Fig. 10, which decouples the optimizations of signal and clock processing. The insets of Fig. 14 show the eye diagrams of the recovered clock and the signal before and after 3R regeneration. The 3R regeneration effectively suppresses the amplitude and time noise on the input signal, and signals with clean eye diagrams are produced for retransmission.

Fig. 15 shows the experimental results of the field trial with 264-km loop length. Fig. 15(c) shows that 3R regeneration maintains the signal eye diagrams in a constant shape through Laps 1 to 1000 (264–264 000-km field transmission) with clear openings. As a comparison, when the 3R regenerator is removed from the recirculation loop, the eye diagrams of the

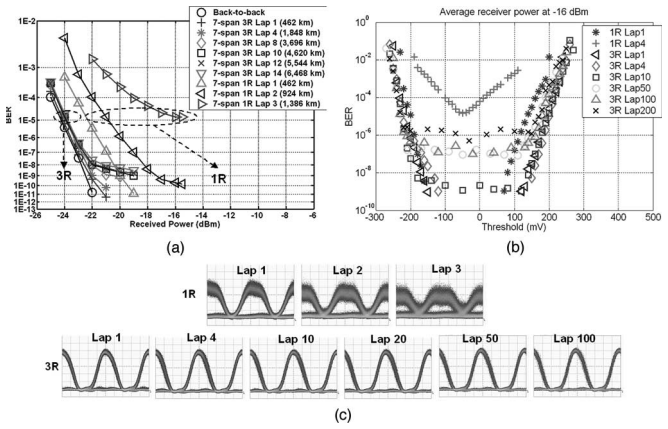

Fig. 16. Experimental results when loop length is 462 km. (a) BER curves. (b) BER versus threshold at −16-dBm receiver power. (c) Eye diagrams.

1R scheme become closed and noisy at Lap 6 (1584 km). The BER curves in Fig. 15(a) indicate that the optical 3R achieves error-free operation ($\mathrm{BER} < 10^{-9}$) at Lap 1000. The BER curves of 3R Lap 1 to Lap 200 overlap that of the back-to-back signal before transmission. At Lap 1000 (after 264 000 km), there is only 1.5-dB power penalty at 10^{-9} BER relative to the back-to-back case. The BER curves of the 1R scheme show an error floor around 10^{-5} at Lap 6. For Lap 1, the 3R scheme achieves a 2-dB negative power penalty at 10^{-9} BER compared to the 1R scheme. The Q-factor plots in Fig. 15(b) also show that the optical 3R slows down the Q degradation and effectively extend the transmission reach.

To investigate the relation between the cascadability and the spacing of the optical 3R, we increase the loop length to 462 km. Fig. 16(c) shows the eye diagrams. The eye diagrams of the 1R scheme exhibit much faster noise accumulation due to the increased loop length. The eye diagram of the 1R scheme closes at Lap 3 (1386 km), while the eye diagrams of the 3R scheme remain clean and open even at Lap 200 (92 400 km). Fig. 16(a) indicates that with 3R, error-free operation can be obtained at Lap 4. Also, the 3R scheme achieves a 2-dB negative power penalty at 10^{-9} BER relative to the 1R scheme at Lap 1. However, the 3R BER curves show bending at Lap 8, and there is an error floor around 10^{-9} at Lap 14. The BER increment is due to the low input OSNR (20.6 dB). Low OSNR makes the overlap between noise distributions associated with mark- and space-levels large and increases the possibility of wrong thresholding conducted by the optical 3R regenerator. The low OSNR also affects the performance of the clock recovery. Without 3R, the 1R BER curves start to bend at Lap 2, and there is an error floor around 10^{-5} at Lap 3. The BER versus threshold plots in Fig. 16(c) shows that the optical 3R effectively slows down the BER increase. The error floor at 3R Lap 200 is between 10^{-5} and 10^{-6}, which is still below the forward-error-correction (FEC) threshold.

The experimental results prove the stable operation of the optical 3R regenerator under relatively realistic conditions. Note that due to the recirculation method, the field-trial experiments only minimize but do not eliminate the ideal conditions. The experiments also reveal the tradeoff between input OSNR and the optical 3R cascadability. The BER measurements indicate that for this optical 3R regenerator, the 3R spacings of 264 and 462 km have comparable performance when the total transmission distance is less than 1848 km.

VI. Summary

In this paper, we first experimentally investigated the limitations of 2R regenerators built with all-active SOA-MZIs. These 2R regenerators can effectively suppress the amplitude domain noise. However, due to the speed limitation from the carrier dynamic and the ASE noise from the active structure, timing-jitter accumulation becomes a major problem and limits the cascadability of such optical 2R regenerators. We then proposed and demonstrated optical 3R techniques for high-performance and scalable 10-Gb/s transmission systems. The optical 3R regenerators relied on narrowband optical filtering using an FPF for optical clock recovery. Several optical 3R configurations using the optical clock-recovery technique were then demonstrated in fiber recirculation loop experiments. With the wavelength conversion in a SOA-MZI, we successfully overcame the polarization dependence of the FPF and achieved stable clock recovery for polarization-scrambled signals after fiber transmission. The experimental demonstration achieved low-penalty error-free 10-Gb/s RZ transmission using PRBS $2^{23}-1$ through a record distance of 1.25 million km across 10 000 3R stages. To overcome the clock RF fading from CD, we proposed and demonstrated an all-optical clock-enhancement technique using a simple configuration of a SOA-MZI. The experimental demonstrations showed error-free 125 000-km 10-Gb/s dispersion uncompensated transmission using PRBS $2^{23}-1$ through 1000 optical 3R stages with the clock enhancement. Field-trial experiments were included to assess the optical 3R regeneration techniques under relatively practical conditions and to investigate the relation between the cascadability and the spacing of the optical 3R. With 264-km SSMF transmission in each loop and 23.5-dB input OSNR, the 3R field experiments demonstrated error-free 10-Gb/s RZ transmission over 264 000-km field fiber using PRBS $2^{23}-1$. There was only 1.5-dB power penalty at 10^{-9} BER after 264 000-km field transmission compared to the back-to-back case before transmission. With a 3R spacing of 462 km and 20.6-dB input OSNR, the 3R regenerator obtained 1848-km error-free transmission, and the BER was far below the FEC threshold, even after 92 400-km field transmission.

References

[1] J. Leuthold, "Signal regeneration and all-optical wavelength conversion," presented at the Lasers and Electro-Optics Soc. Conf. (LEOS), Glasgow, U.K., Nov. 2002, Paper MM1.

[2] O. Leclerc *et al.*, "Optical regeneration at 40 Gb/s and beyond," *J. Lightw. Technol.*, vol. 21, no. 11, pp. 2779–2790, Nov. 2003.

[3] M. Karlsson *et al.*, "PMD compensation using 2R and 3R regenerators," presented at the Eur. Conf. Optical Commun. (ECOC), Glasgow, U.K., Sep. 2004, Paper We1.4.2.

[4] A. Dupas *et al.*, "2R all-optical regenerator assessment at 2.5 Gb/s over 3600 km using only standard fibre," *Electron. Lett.*, vol. 34, no. 25, pp. 2424–2425, Dec. 1998.

[5] P. Ohlen *et al.*, "Noise accumulation and BER estimates in concatenated nonlinear optoelectronic repeaters," *IEEE Photon. Technol. Lett.*, vol. 9, no. 7, pp. 1011–1013, Jul. 1997.

[6] J. Mork *et al.*, "Analytical expression for the bit error rate of cascaded all-optical regenerators," *IEEE Photon. Technol. Lett.*, vol. 15, no. 10, pp. 1479–1481, Oct. 2003.

[7] J. Leuthold *et al.*, "40 Gb/s transmission and cascaded all-optical wavelength conversion over 1 000 000 km," *Electron. Lett.*, vol. 38, no. 16, pp. 890–892, Aug. 2002.
[8] G. Raybon *et al.*, "40 Gb/s pseudo-linear transmission over one million kilometers," presented at the Optical Fiber Commun. Conf. (OFC), Anaheim, CA, Mar. 2002, Paper FD10.
[9] B. Sartorius *et al.*, "System application of 40 GHz all-optical clock in a 40 Gb/s optical 3R regenerator," presented at the Optical Fiber Commun. Conf. (OFC), Baltimore, MD, Mar. 2000, Paper PD11.
[10] B. Lavigne *et al.*, "Performance and system margins at 10 Gb/s of optical repeater for long haul NRZ transmission," presented at the Eur. Conf. Optical Commun. (ECOC), Madrid, Spain, Sep. 1998, Paper 559–560.
[11] C. Joergensen *et al.*, "All-optical wavelength conversion at bit rates above 10 Gb/s using semiconductor optical amplifiers," *IEEE J. Sel. Topics Quantum Electron.*, vol. 3, no. 5, pp. 1168–1180, Oct. 1997.
[12] P. Ohlen *et al.*, "Measurements and modelling of pattern-dependent BER and jitter in reshaping optoelectronic repeaters," *Proc. Inst. Electr. Eng.—Optoelectron.*, vol. 147, no. 2, pp. 97–103, Apr. 2000.
[13] R. Pedersen *et al.*, "WDM cross-connect cascade based on all-optical wavelength converters for routing and wavelength slot interchanging using a reduced number of internal wavelengths," presented at the Optical Fiber Commun. Conf. (OFC), San Diego, CA, Mar. 1998, Paper TuJ2.
[14] R. Stephens, "Analyzing jitter at high data rates," *IEEE Commun. Mag.*, vol. 42, no. 2, pp. 6–10, Feb. 2004.
[15] M. Funabashi *et al.*, "All-optical 3R regeneration in monolithic SOA-MZI to achieve 0.4 million km fiber transmission," presented at the Lasers and Electro-Optics Soc. Conf. (LEOS), Sydney, Australia, Oct. 2005, Paper MM3.
[16] Z. Zhu *et al.*, "10 000-hop cascaded in-line all-optical 3R regeneration to achieve 1 250 000 km 10 Gb/s transmission," *IEEE Photon. Technol. Lett.*, vol. 18, no. 5, pp. 718–720, Mar. 2006.
[17] G. Contestabile *et al.*, "A novel 40 Gb/s NRZ all-optical clock recovery," presented at the Conf. Lasers and Electro-Optics (CLEO), Baltimore, MD, May 2005, Paper CMZ2.
[18] M. Jinno *et al.*, "Optical tank circuits used for all-optical timing recovery," *IEEE J. Quantum Electron.*, vol. 28, no. 4, pp. 895–900, Apr. 1992.
[19] B. Lavigne *et al.*, "Improvement of regeneration capabilities in semiconductor optical amplifier-based 3R regenerator," presented at the Optical Fiber Commun. Conf. (OFC), San Diego, CA, Feb. 1999, Paper TuJ3.
[20] F. Devaux *et al.*, "Simple measurement of fiber dispersion and of chirp parameter of intensity modulated light emitter," *J. Lightw. Technol.*, vol. 11, no. 12, pp. 1937–1940, Dec. 1993.
[21] Z. Pan *et al.*, "Chromatic dispersion monitoring and automated compensation for NRZ and RZ data using clock regeneration and fading without adding signaling," presented at the Optical Fiber Commun. Conf. (OFC), Anaheim, CA, Mar. 2001, Paper WH5.
[22] Z. Zhu *et al.*, "1000 cascaded stages of optical 3R regeneration with SOA-MZI based clock enhancement to achieve 10 Gb/s, 125 000 km dispersion uncompensated transmission," *IEEE Photon. Technol. Lett.*, vol. 18, no. 20, pp. 2159–2161, Oct. 2006.

Zuqing Zhu (S'01) received the B.S. degree from the Department of Electronic Engineering and Information Science, University of Science and Technology of China, Hefei, China, in 2001 and the M.S. degree from the Department of Electrical and Computer Engineering, University of California, Davis, in 2003. He is currently working toward the Ph.D. degree at the Department of Electrical and Computer Engineering, University of California, Davis.

His research focuses on the advanced optical switching and regeneration technologies for the next-generation optical networks.

Mr. Zhu is a Student Member of the Optical Society of America (OSA).

Masaki Funabashi received the B.E. and M.E. degrees in electronic engineering from the University of Tokyo, Tokyo, Japan, in 1995 and 1997, respectively.

In 1997, he joined Yokohama R&D Laboratories, The Furukawa Electric Co., Ltd., Yokohama, Japan, where he has been engaged in the research and development of long-wavelength semiconductor optical devices, such as distributed feedback lasers, pump lasers, modulators, and waveguide photodiodes. From 2004 to 2006, he spent two years at the Department of Electrical and Computer Engineering, University of California, Davis, as a Visiting Researcher, where he studied optical signal regeneration and optical-label switching technologies. His research interests include the physics, design, fabrication, and characterization of semiconductor optical devices and their integration and packaging technologies.

Zhong Pan (S'01) received the B.S. degree from Tsinghua University, Beijing, China, in 2000 and the M.S. degree from University of California, Davis (UC Davis), in 2002, both in electrical engineering. He is currently working toward the Ph.D. degree at UC Davis.

His research focuses on optical-label switching in optical communication networks, especially the control of the tunable laser and its application.

Mr. Pan is a Student Member of the Optical Society of America (OSA).

Loukas (Lucas) Paraschis (M'02) was born in Athens, Greece. He received the M.S. and Ph.D. degrees from Stanford University, Stanford, CA, in 1998 and 1999, respectively.

He is a Technical Leader with the Core Routing at Cisco Systems, San Jose, CA, where he is responsible for the next-generation optical technologies, R&D, and network architectures. With Cisco, he has primarily worked on WDM networks, multiservice metro and IP-over-WDM architectures, network availability, and techno-economical analysis. Prior to Cisco, he worked as an R&D Engineer. He has coauthored more than 35 peer-reviewed technical publications, multiple invited, keynote, and tutorial presentations, technical reports, and three patent disclosures.

Dr. Paraschis has been the Editor for optical networks of *Journal of Communications and Networks*, Guest Coeditor for the JOURNAL OF LIGHTWAVE TECHNOLOGY (Nov. 2004), Panelist of the National Science Foundation (NSF), and a member of conference organizing committees and SPIE.

David L. Harris (M'98), photograph and biography not available at the time of publication.

S. J. Ben Yoo (S'82–M'84–SM'97–F'06) received the B.S. degree in electrical engineering (with distinction), the M.S. degree in electrical engineering, and the Ph.D. degree in electrical engineering with minor in physics from Stanford University, Stanford, CA, in 1984, 1986, and 1991, respectively.

Prior to joining Bellcore in 1991, he conducted research on nonlinear optical processes in quantum wells, a four-wave mixing study of relaxation mechanisms in dye molecules, and ultrafast diffusion-driven photodetectors. During this period, he also conducted research on lifetime measurements of inter-subband transitions and on nonlinear optical storage mechanisms with Bell Laboratories and IBM Research Laboratories, respectively. Prior to joining the University of California, Davis (UC Davis) in 1999, he was a Senior Research Scientist with Bellcore, leading technical efforts in optical networking research and systems integration. His research activities with Bellcore included optical label switching for the next-generation Internet, power transients in reconfigurable optical networks, wavelength interchanging crossconnects, wavelength converters, vertical-cavity lasers, and high-speed modulators. He also participated in the advanced technology demonstration network/multiwavelength optical networking (ATD/MONET) systems integration, the OC-192 synchronous optical network (SONET) ring studies, and a number of standardization activities. He is currently a Professor of electrical engineering with UC Davis and the Director of UC Davis branch Center for Information Technology Research in the Interest of Society (CITRIS). His research at UC Davis includes unified heterogeneous networking and high-performance routing systems for next-generation networks. In particular, he is conducting research on architectures, systems integration, and network experiments related to all-optical label switching routers and optical code division multiple access technologies.

Prof. Yoo is a Fellow of IEEE Lasers and Electro-Optics Society (LEOS) and a Fellow of the Optical Society of America (OSA) and a member of Tau Beta Pi. He also serves as Associate Editor for IEEE PHOTONICS TECHNOLOGY LETTERS and served as Guest Editor for IEEE/OSA JOURNAL OF LIGHTWAVE TECHNOLOGY Special Issue on Optical Networking in 2005. He was the recipient of the DARPA Award for Sustained Excellence in 1997, the Bellcore CEO Award in 1998, and the Mid-Career Research Faculty Award (UC Davis) in 2004.